Physics Letters B 841 (2023) 137935

Contents lists available at ScienceDirect

Physics Letters B

journal homepage: www.elsevier.com/locate/physletb

Hunting for an EMC–like effect for antiquarks

Massimiliano Alvioli [a,b,*], Mark Strikman [c]

[a] Consiglio Nazionale delle Ricerche, Istituto di Ricerca per la Protezione Idrogeologica, via Madonna Alta 126, I-06128, Perugia, Italy
[b] Istituto Nazionale di Fisica Nucleare, Sezione di Perugia, via Pascoli 23c, I-06123, Perugia, Italy
[c] 104 Davey Lab, The Pennsylvania State University, University Park, PA 16803, USA

ARTICLE INFO

Article history:
Received 29 October 2022
Received in revised form 16 April 2023
Accepted 23 April 2023
Available online 27 April 2023
Editor: J.-P. Blaizot

ABSTRACT

We argue that the Drell–Yan process in the $x_A \geq 0.15$ kinematics recently studied at FNAL by the E906/SeaQuest experiment may allow to observe an analogous of the EMC effect for antiquarks. The effects of Fermi motion and energy loss are considered. The preliminary E906/SeaQuest data are inconsistent with the growth of the $\sigma_A/A\sigma_N$ ratio expected in the Fermi motion scenario at $x_A \geq 0.25$. The pattern of the x_A dependence of the ratio seems also inconsistent with a scenario in which the dominant nuclear effect is a suppression of the cross section due to the energy loss experienced by a quark of the projectile proton involved in the Drell–Yan process. All together the data suggest the possibility of a modification of the antiquark parton distributions in nuclei, with a pattern similar to the one observed in the EMC effect. We argue that optimal kinematics to look for an antiquark EMC–like effect would be to measure the $\sigma_A^{DY}/A\sigma_N^{DY}$ ratios for x_A = 0.2 – 0.4 and $x_p \approx$ constant.

1. Introduction

Forty years ago the European muon collaboration (EMC) [1] has found that the quark parton distributions in nuclei at $x \geq 0.4$ are substantially different from the expectations from the impulse approximation, which includes Fermi motion effects. For example, the ratio of structure functions F_2:

$$R_A(x, Q^2) = \frac{F_{2A}(x, Q^2)}{Z\, F_{2p}(x, Q^2) + N\, F_{2n}(x, Q^2)}, \quad (1)$$

for μA scattering is about 0.9 at $x \sim 0.5$ for $A \geq 12$, $Q^2 \geq$ few GeV^2. This pattern (the EMC effect) is inconsistent with the expectations from models in which the conservation of baryon, electric charge, and momentum distribution sum rules are implemented [2], and non–nucleonic degrees of freedom are neglected; see also the discussion in section 2.

Over the years a number of searches have been performed, looking for deviations of R_A from unity for different parton densities outside the nuclear shadowing region $x \leq 0.01$. No significant deviations were observed for antiquarks in the region $0.05 \leq x \leq 0.15$ (for a review see [8]), in which they were expected in the pion models of the EMC effect (see discussion in Ref. [3]). Precision data from the new muon collaboration (NMC) [4] also show a minuscular ($\sim 3\%$) enhancement of the valence quarks in the same x range and $A = 40$. This enhancement appears to be mostly due to the conservation of the number of valence quarks (the baryon sum rule). In the gluon channel, the momentum sum rule in combination with the gluon shadowing data suggests an enhancement at $x \sim 0.1$ [3]. Also the large hadron collider (LHC) forward dijet production data [5] are in a better agreement with the models assuming the existence of an EMC–like effect for gluons at $x \sim 0.5$ than with models assuming that the nuclear gluon density is not modified for these values of x. Still, studies of dijet production do not allow to measure directly an EMC effect for gluons, since in the $x \sim 0.5$ kinematics the gluon contribution is a small correction to the quark contribution, which is known at large Q^2 and $x = 0.5$ due to large errors of the measurements of $F_{2A}(x, Q^2)$ in this kinematics.

Recently, a new series of measurements of the Drell–Yan (DY) process have been performed by the E906/SeaQuest collaboration at Fermi Lab using an injector proton beam of the energy 120 GeV [6,7]. The data covered a wide range of x_A and x_p for the target antiquarks, up to x_A = 0.45. The experiment also studied the A–dependence of the DY cross section. Thus, in principle, these data allow to measure the antiquark ratio in a much wider x range than the data obtained at the Tevatron [8].

Muon pair production data from E906/SeaQuest show a substantial difference in up and down antiquark distributions [9], with larger distributions for down than up antiquarks, over a wide range of momenta. Global analyses of parton distribution functions now include E906/SeaQuest data, which helped reducing significantly

* Corresponding author.
E-mail address: massimiliano.alvioli@irpi.cnr.it (M. Alvioli).

https://doi.org/10.1016/j.physletb.2023.137935

the uncertainties of $\bar{d}/\bar{u}$ at large x [10]. The observation of a flavor asymmetry for antiquarks may have consequences for the existence of an EMC effect for antiquarks.

Since the antiquark distributions in the nucleon drops very rapidly with increasing x, one may expect that deviations from a Fermi motion model of nuclear effects may show up at smaller x than for quarks, where a significant effect is observed only for $x \geq 0.45$; see Section 2. We stress that EMC–like effects for antiquarks may be present in a number of different models.

For example, the QCD radiation model [11,12] assumes that the size of a bound nucleon is larger than that of a free nucleon, and the QCD evolution starts at values of Q^2 inversely proportional to the radius of the bound nucleon. As a result, the model predicts a suppression of quarks, antiquarks and gluons distributions at large x. Another model [3,13] starts from the observation that a bound nucleon in a small size configuration interacts with smaller attraction with the nearby nucleons due to color transparency, resulting in a reduction of the probability of such configurations. To relate this effect to the EMC effect, the authors argue that the configurations including a leading large–x parton with a small size. In the case of valence quarks, this conjecture is supported by the analysis of the LHC and RHIC pA and dA dijet production data [14,15].

Overall, the observation of nuclear modification of a second nuclear parton density would provide a strong boost to the theoretical and experimental studies of non–nucleonic degrees of freedom in nuclei.

Hence, in Section 2, we explore what kinematics is optimal for distinguishing between the Fermi motion effect and possible effects of non–nucleonic degrees of freedom in nuclei. In section 3 we also compare the A–dependence of the DY process due to possible energy loss experienced by quarks propagating through the nucleus and due to non–nucleonic degrees of freedom, and find them substantially different. Moreover, we point out that in the kinematics $x_p \sim 0.8, x_A \sim 0.2$ the energy loss effect should be much larger than for $x_p \sim 0.2, x_A \sim 0.4$. Thus, combined studies of the nuclear effects in these kinematics would allow to look for an EMC effect for antiquarks in nuclei in a more constrained way.

2. Fermi motion effect for antiquarks

To observe an EMC effect for antiquarks one needs to find the optimal x–range where Fermi motion effects are small as compared to potential effects of the existence of non–nucleonic degrees of freedom. Since parton densities represent the light cone projection of the hadron wave function, we need to use light cone nuclear wave functions [2]. Similar to the case of quark and gluon parton distribution functions, see *e.g.* [16], we introduce the light cone single nucleon density matrix: $\rho_A^N(\alpha)$. Here α/A is the fraction of the momentum of the fast nucleus, P_A, carried by a nucleon, with $0 \leq \alpha \leq A$. It can be interpreted as the probability to find a nucleon having longitudinal momentum $\alpha P_A/A$. Considering the matrix element of the baryon current at $t = 0$, one finds:

$$\int \rho_A^N(\alpha)\,\frac{d\alpha}{\alpha} = A\,, \tag{2}$$

while the sum rule

$$\frac{1}{A}\int \alpha\,\rho_A^N(\alpha)\,\frac{d\alpha}{\alpha} = 1 \tag{3}$$

follows from considering the energy–momentum tensor sum rule, basically from the condition that the sum of the light cone fractions of A nucleons is equal to unity.

The effect of Fermi motion can be written in terms of nuclear parton distributions in complete analogy with the QCD evolution equations:

$$x\,p_A(x) = \int \rho_A^N(\alpha)\,\frac{x}{\alpha}\,p_N\left(\frac{x}{\alpha}\right)\,\frac{d\alpha}{\alpha}\,, \tag{4}$$

where we do not write explicitly the dependence of the parton densities on Q^2. Since the spread of the momentum distribution over the light cone fraction α is pretty modest, we can consider a Taylor series expansion using $1-\alpha$ as a small parameter. We obtain, after applying the sum rules in Eqs. (2) and (3):

$$R_A(x) = 1 + \frac{x^2\,(x\,p_N(x))'' + 2\,x(x\,p_N(x))'}{x\,p_N(x)}\,\frac{T_A}{3\,m_N}\,. \tag{5}$$

In the last step of Eq. (5), we substituted $\int \frac{d\alpha}{\alpha}(1-\alpha)^2$ with its non–relativistic limit, $T_A/3$, where T_A is the nucleon average kinetic energy. For a detailed discussion, see Ref. [3].

To see the pattern given by Eq. (5) we can use the parametrization:

$$x\,p_N(x) \propto (1-x)^n\,, \tag{6}$$

where $n \approx 3$ for quarks and $n \approx 7$ for antiquarks; thus, we obtain:

$$R_A(x) = 1 + \frac{x\,n\,[x\,(n+1)-2]}{(1-x)^2}\,\frac{T_A}{3m_N}\,. \tag{7}$$

It follows from Eq. (7) that the contribution of Fermi motion passes through zero at the crossover point, x_{cr}:

$$x_{cr} = \frac{2}{n+1}\,, \tag{8}$$

that is, $x_{cr} = 0.5$ for $n = 3$ (quarks), and $x_{cr} = 0.25$ for $n = 7$ (antiquarks). For $x < x_{cr}$, R_A reaches the minimum at $x = 1/n$, where

$$R_A\left(\frac{1}{n}\right) = 1 - \frac{n}{n-1}\,\frac{T_A}{3m_N}\,. \tag{9}$$

Assuming $T_A = 40$ MeV, for illustration, (using $T_A = \int d\boldsymbol{k}\,k^2/(2m_N)\,n_A(k)$ we have $T_A = 30.35$ MeV for carbon, and $T_A = 36.75$ MeV for iron, with the momentum distribution adopted here), we find that the deviation from unity of R_A for antiquarks expected from the Fermi motion model to be of the order 1.5% for $x_A \sim 0.1$.

Hence $x_A \sim 0.2$ – 0.3 is the optimal x–range to suppress the contribution of Fermi motion into R_A for antiquarks. We checked that Eq. (7) is a good approximation to the convolution expression. For simplicity we considered a model in which, for $k \leq k_F$, the non–relativistic momentum distribution, $n_A(k)$, is constant. For $k > k_F$ we used the two–nucleon short range correlation approximation with high momentum tail enhanced by a factor $a_2 \approx 4$ as compared to the deuteron wave function. The value of $n_A(k)$ for $k < k_F$ was determined from normalization condition $\int n_A(k)\,d\boldsymbol{k} = 1$. The resulting $n_A(k)$ is presented in Fig. 1. Obviously one can use a more sophisticated model including the motion of the short range correlations in a mean field [17–20]; for a recent review see Ref. [21]. However, this seems not necessary since these effects constitute a small correction to an already small effect. To ensure that the momentum sum rule is fulfilled, we used the two–nucleon relation valid for the deuteron for any value of k. Hence, for the two–nucleon short range contribution:

$$\alpha = 1 + \frac{k_3}{\sqrt{k^2 + m_N}}\,. \tag{10}$$

In this approximation:

$$x\,p_N(x) = \int \frac{x}{\alpha}\,x\,p_N\left(\frac{x}{\alpha}\right)\,n_A(k)\,d\boldsymbol{k}\,. \tag{11}$$

The results of calculations of the approximate and full convolution formulae are compared in Fig. 2; full details of calculations

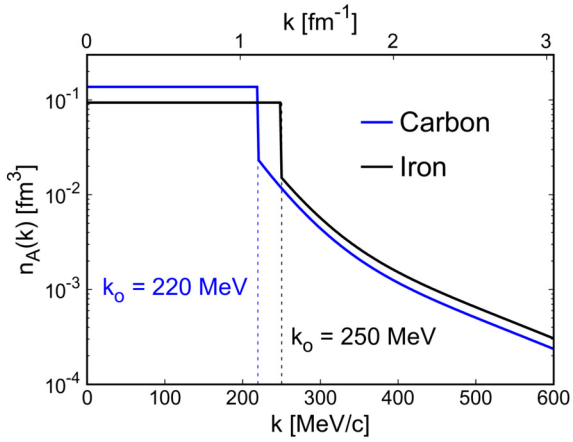

Fig. 1. The piecewise momentum distribution of Eq. (17), for two nuclei considered here and in Fig. 2. The curves are normalized as $\int d\boldsymbol{k} n_A(k) = 1$.

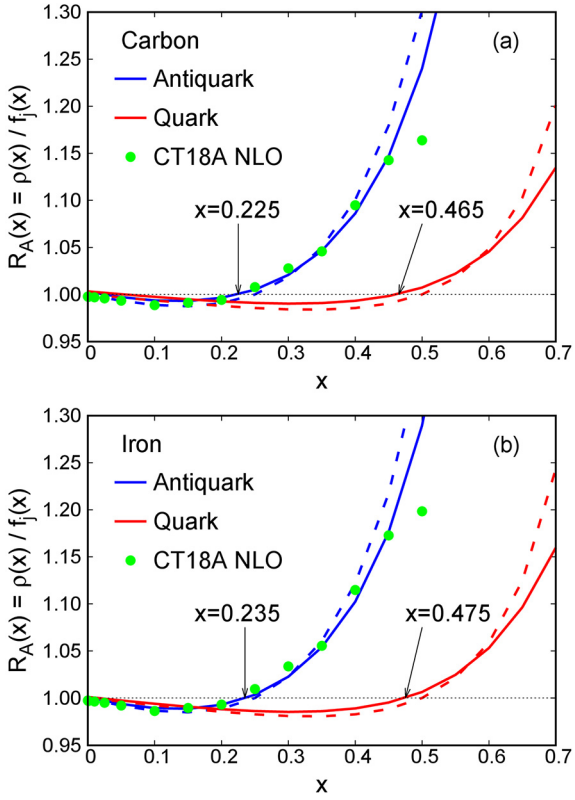

Fig. 2. Results for the ratio of the convolution formula, Eq. (21), for (a) k_0 = 220 MeV = 1.115 fm^{-1} (carbon), and (b) k_0 = 250 MeV = 1.270 fm^{-1} (iron); in both cases, a_2 = 4. Dashed lines correspond to the Taylor series expansion of Eq. (7). For antiquarks, green circles show the calculations using CT18A NLO PDFs [22], instead of the approximate PDFs of Eq. (6).

are presented in Appendix A. One can see that the agreement is very good in the region of interest, with $R_A^{\bar{q}}$ becoming significantly larger than unity already at x = 0.4. The figure also shows results obtained using antiquarks distribution functions CT18A NLO [22], instead of the approximate PDFs of Eq. (6). The results, including the crossing point, are not appreciably different, in the considered x range.

In the case of the x–dependent ratio, Fig. 2, we wanted to emphasize the effect of Fermi motion in a particular nucleus and thus presented the ratio of cross section of DY cross sections on a nucleus and on a free nucleon. Experimentally one usually measures the nucleus/deuteron ratio. The Fermi motion effect in the discussed x–range is proportional to the average kinetic energy of the nucleon (see *e.g.* Eq. (5)) which in turn is roughly proportional to $a_2(A)$. So for $A \sim 40$, where $a_2 \sim 5$, the Fermi motion correction is reduced by about 20%.

3. Energy loss mimicking EMC effect

A quark propagating through a nucleus may interact with the nuclear medium, resulting in an energy loss. Such an energy loss would reduce the cross section for a given x_p, thus mimicking an EMC–like effect. Since the gluon density the parton travels through is pretty modest, this effect should be proportional to the average gluon density a quark traveled through.

We developed a Monte Carlo model to estimate the A–dependence of this effect. The positions of nucleons (configurations) were generated using the algorithm of [23–25]. The position of the hard interaction point was generated based on the gluon distributions in individual nucleons, and the gluon transverse density was generated for each event (*i.e.*, for each configuration) using information about gluon generalized distribution in nucleons based on the analysis of the J/ψ exclusive photoproduction [14,15]. We also assumed that the longitudinal distribution of gluons in nucleons is the same as a transverse one. This was a minor effect relevant to generating longitudinal position of the interaction point and considering the propagation of quark through the gluon field generated by nearby nucleons. Fig. 3 shows a sketch of the process described here, illustrating the nucleons contributing to the gluon density traveled through by the quark, for sample hard interactions located at different points along the direction of propagation. Additional details of the calculations are given in Appendix B.

Our calculation gives the A–dependence of the deviation of $R_A^{\bar{q}}(x)$ from unity: $Z_H = c\,(1 - R_A^{\bar{q}})$, where the universal factor c depends on the absolute rate of the energy loss. The results of calculation are presented in Fig. 4, where we used a normalization factor $c = 1$. Since the experiment reports data for the nucleus/deuteron ratios rather than nucleus/free nucleon ratios, the figure shows the result of the calculation for the deuteron as well. As expected, account of the spatial correlations between nucleons leads to a very small effect. We also show in Fig. 4 the A–dependence corresponding to simple geometry: $Z_H \propto A^{1/3}$ normalized to the value of Z_H for A = 12.

The natural question is whether one can distinguish the EMC like effect and the energy loss effect, studying the A–dependence of the deviation of $R_A(x)$ from unity. We will restrict the discussion about this point to two of the nuclei studied by the E906/SeaQuest collaboration, carbon and copper, since in these cases the isospin effects are small, while it may not be the case for tungsten, for an EMC–like effect.

Fig. 4 shows the A–dependence of energy loss effects, which can be studied comparing the x–dependence of the EMC ratio or its x–slope, dR_{EMC}/dx in the x–range $0.2 < x < 0.5$, where the EMC effect depends linearly on x; for recent studies see [26] and references therein. Using a linear fit of the EMC slope presented in Fig. 23 of Ref. [26], we considered the ratio of the EMC slope for copper over carbon, and estimated:

$$G_{Cu/C} = \frac{dR_{Cu}/dx}{dR_C/dx} = 1.35\,. \tag{12}$$

In the region of x = 0.5 – 0.6, where the EMC effect reaches the maximum, and one cannot use a linear fit, so we can compare $R_A(x) - 1$ using the data of [27]. They are consistent with the observation, repeated several times, that the shape of $R_A(x) - 1$ is practically A–independent for $0.1 < x \leq 0.7$; see references in Ref. [3].

It was observed in the studies summarized in Ref. [21] that the EMC effect is proportional to the probability of two nucleon short

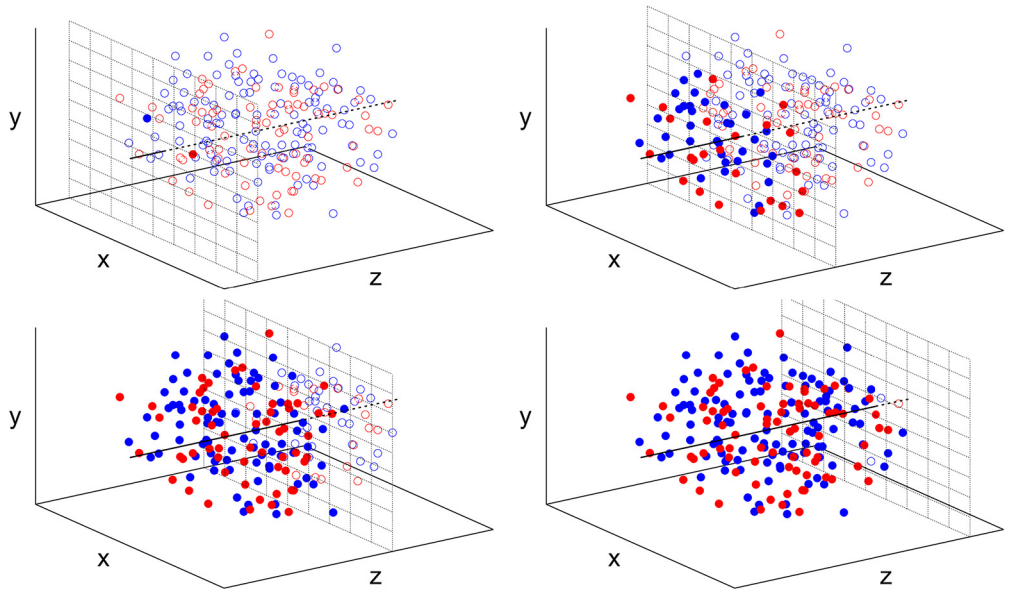

Fig. 3. A sketch of the procedure described in Section 3 and in Appendix B. The figure represents with full circles the nucleons involved in the summation of Eq. (23), and with empty circles the nucleons left out of the summation, for a given distance traveled in the z direction by the quark in the nuclear medium (red/blue are protons/neutrons). Such distance corresponds to the hard interaction point, calculated as in [14,15]; we show four examples, for one given configuration of the gold nucleus.

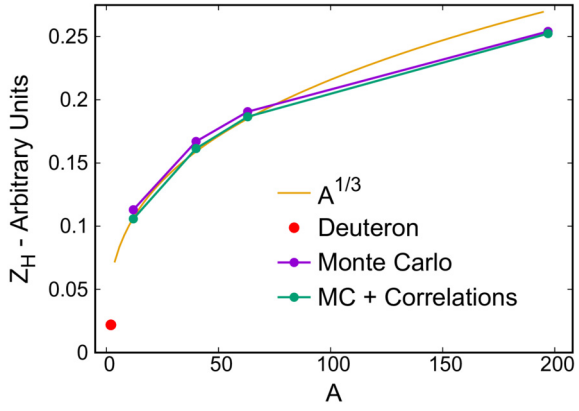

Fig. 4. A–dependence of the energy loss effect discussed in Section 3. The figure shows results for Z_H, defined as the ratio of Eq. (23) in Appendix B.

range correlations in nuclei. A well–known quantity used to show the scaling behavior of short range correlations as a function of A is $a_2(A)$, the ratio of quasielastic cross sections with nuclear targets to the corresponding cross section on the deuteron, at $x > 1.3$ [3,28–30]. Using values of $a_2(A)$ reported in [31], one predicts a weaker increase of the EMC effect between carbon and copper than given by Eq. (12): $(R_{Cu} - 1)/(R_C - 1) \sim 1.2$. However, the value estimated in Eq. (12) involved directly the DIS data for A/D ratios, and the discrepancy is likely to be within the statistical confidence interval. Also, the methods used to account for Fermi motion of the $2N$ pair (and, hence, the values of $a_2(A)$) are different, in different analyses.

The ratio we found based on the ad hoc, but reasonable, assumption that EMC effect for antiquarks and for quarks are similar, leads to a much weaker A–dependence than the energy loss mechanism, which gives:

$$G_{Cu/C}^{en.loss} = \frac{R_{Cu} - 1}{R_C - 1} = 1.86\,. \tag{13}$$

Assuming that the magnitude of nuclear effect is similar to the effect for quarks, about 10%, we conclude that the value of the A_1/A_2 ratio on the scale of 1% reached in the previous DY experiments would be able to distinguish reliably the two mechanisms. Extra discrimination is possible using the lightest nuclei (^{4}He, ^{6}Li), for which the energy loss effect is very small, while the EMC effect is already significant. Still it would be a challenging measurement, since the EMC effect for ^{4}He does not typically exceed 5%.

Another approach to probe the role of the energy loss mechanism in the DY process (probably more promising) would be to study the dependence of the A/D ratio on x_p, as a function of x_A. In the kinematics of the E906/SeaQuest experiment, one considers $M^2(\mu\mu) = x_p \cdot x_A s$ close to the cutoff from below on the mass of the DY pair of ~ 4 GeV. The energy loss of the quark is commonly assumed to be a weak function of its momentum, hence the suppression of the cross section should be:

$$\frac{\sigma}{\sigma_{IA}} = \frac{(1 - x_p - \Delta)^N}{(1 - x_p)^N} \approx 1 - \frac{N\Delta}{(1-x)}\,, \tag{14}$$

where IA stands for impulse approximation. In Eq. (14) we used $(1 - x_p)^N$ for the quark distribution, and Δ is the ratio of energy loss and the projectile momentum. For x_A = 0.1, x_p = 0.8, and x_A = 0.25, x_p = 0.32, the suppression differs by a factor 0.68/0.2 = 3.4. Hence, the energy loss would result in a strongest suppression of the A/D ratio at the smallest $x_A \sim 0.1$. The preliminary E906/SeaQuest data do not indicate such a pattern. Moreover, the high energy data [8]) for which the energy loss effects should be much smaller, do not observe any modification of antiquark distributions in nuclei except for nuclear shadowing, within 2% accuracy for $x \leq 0.15$.

Hence, we also performed a direct comparison with preliminary data presented in Ref. [7]. We considered data in the smallest x_A data bin, $x_A \in [0.1, 0.13]$), as for 0.1 to 0.13 larger values of x_A the effect of energy loss is expected to be smaller; see discussion above. The data shows the ratio $R(A/D)$, extracted from the ratio of the cross section for three target nuclei (carbon, iron and tungsten) to the cross section with a target deuteron. We compared the three data points with the estimated ratio $R(A/D)$, obtained from the ratio of the energy loss in the nucleus and the deuteron scattering, $Z_H(A)/Z_H(D)$, as follows:

$$R(A/D) = 1 - k\, Z_H(A)/Z_H(D)\,, \tag{15}$$

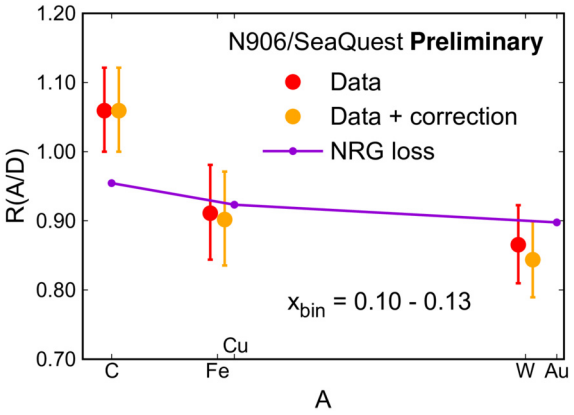

Fig. 5. A–dependence of preliminary E906/SeaQuest data. Red circles are the published data [7], yellow circles are data including the isoscalar correction of Eq. (27) in Appendix C. Symbols corresponding to data and corrected data were displaced horizontally for clarity of presentation. The purple curve is the energy loss scenario estimate for the ratio $R(A/D)$, obtained from Eq. (15).

where k is a parameter fitted to the three existing data points, and Z_H is the quantity in Fig. 5. The model calculations of the energy loss effect considered copper and gold target nuclei, instead of iron and tungsten, used in the experiment. A linear interpolation of the data points along the A direction to obtain values for A actually used in the simulations produced indistinguishable results.

Fig. 5 indicates that the estimated A dependence of the energy loss effect does not contradict the data in the smallest x bin, though errors are pretty large, and the data point for carbon case exceeds 1, which is impossible in the energy loss mechanism. Thus, based on Eq. (14) and the $x \sim 0.1$ data, we expect that for the $x_A \geq 0.3$ the modification of the cross section due to energy loss should not exceed 2 – 3%, even for heavy nuclei (this estimate is now mainly limited by the current error bars of the data).

4. Conclusions

We performed an extensive analysis of the Fermi motion and energy loss effects in the kinematics of E906/SeaQuest experiment. The PhD thesis of Ref. [7] based on the analysis of a subset of the E906/SeaQuest DY data concluded that "although limited by statistical uncertainty, the ratio R_{pA} may begin to gradually drop off at $x_A \sim 0.25$ but is statistically consistent with 1".

Our analysis indicates that such a pattern is unlikely to originate from the energy loss experienced by the quarks traveling through the nuclear medium. Moreover, we have shown that in the absence of an EMC–like effect the highest x_A data points should exhibit a strong upward trend, which was not observed, and an overall growth starting at $x \sim 0.25$; see Fig. 2. This suggests a similar pattern to the EMC effect for quarks, except that the suppression is starting at much smaller x_A and that Fermi motion enhancements starts at $x \geq 0.3$ rather than at $x \sim 0.8$ for F_{2A}/F_{2D}. Future data analyses would benefit from separating the x_p and x_A dependencies, especially for large x_p. Data for different incident proton energies would be of help as well.

We are eagerly awaiting for the final results of E906/SeaQuest for the A–dependence of the DY process, and for further experimental studies of the DY process in this x_A range for at several incident proton energies.

Declaration of competing interest

The authors declare that they have no known competing financial interests or personal relationships that could have appeared to influence the work reported in this paper.

Data availability

The authors do not have permission to share data.

Acknowledgements

We thank L. Frankfurt for useful discussions during the preparation of the manuscript. Special thanks go to the members of the E906/Sea Quest collaboration, especially to D. Geesaman and A.S. Tadepalli, for very useful comments and questions. M.S.'s research was supported by the US Department of Energy Office of Science, Office of Nuclear Physics under Award No. DE–FG02–93ER40771.

Appendix A

We consider Fermi motion effect using the following expression:

$$f(x, Q^2) = \int d^3k\, n_A(k)\, f_j(x/\alpha, Q^2)\,, \tag{16}$$

where $n_A(k)$ is the momentum distribution, which we define piecewise, as follows:

$$n_A(k) = \begin{cases} C\,, & k \leq k_o\,; \\ \lambda\, a_2\, |\Psi_D(k)|^2\,, & k > k_0\,. \end{cases} \tag{17}$$

In Eq. (17), we used k_0 = 220 MeV = 1.115 fm^{-1}, for carbon, and k_0 = 250 MeV = 1.270 fm^{-1}, for iron; a_2 = 4 for both nuclei. For the deuteron wave function, in Eq. (17), we used results from the AV18 potential interaction [32]. The momentum distribution of Eq. (17) is normalized as $\int n_A(k)\, d\boldsymbol{k} = 1$, and it is shown in Fig. 1. We first calculate the normalization for $k < k_0$ [17,18], to obtain C:

$$0.8 = \int d\boldsymbol{k}\, n_A(k) = 4\pi \int_0^{k_0} k^2 dk\, C\,; \tag{18}$$

we obtained C = 0.1378 for carbon and C = 0.094 for iron.

Then we calculate the normalization for $k > k_0$, to obtain λ:

$$\begin{aligned} 0.2 &= \int d\boldsymbol{k}\, n_A(k)\, \delta(k - k_0) \\ &= 2\pi \int_0^\infty k_\perp dk_\perp \int_{-\infty}^\infty dk_3\, \lambda\, a_2\, |\Psi_D(k)|^2\, \delta(k - k_0)\,, \end{aligned} \tag{19}$$

where $n_A(k)$ depends on k modulus only, but we integrate in $dk_3\, dk_\perp$ because when we insert $f(x/\alpha)$ we have dependence on both k_3 and $k_\perp$. From Eq. (19), we obtained λ = 0.7764 for carbon and λ = 1.0022 for iron.

Eventually, we calculate the quantity of interest as:

$$\begin{aligned} f(x, Q^2) &= \int d\boldsymbol{k}\, n_A(k)\, f_j(x/\alpha, Q^2) \\ &= 2\pi \int_0^\infty k_\perp dk_\perp \int_{-\infty}^\infty dk_3\, n_A(k)\, f_j(x/\alpha, Q^2)\,, \end{aligned} \tag{20}$$

with $k = \sqrt{k_\perp^2 + k_3^2}$, $f_j(x, Q^2) = (1 - x)^n$, n = 7 for $j = \bar{q}$ and n = 3 for $j = q$, and $\alpha = 1 + \frac{k_3}{\sqrt{m^2 + k^2}}$. Now we define the left hand side of Eq. (20) as $\rho(x)$, for given Q^2, and we calculate the ratio:

$$R_A(x) = \rho(x)/f_j(x) = \frac{\int d\boldsymbol{k}\, n_A(k)\, f_j(x/\alpha)}{f_j(x)}\,. \tag{21}$$

Fig. 2 shows the ratio of Eq. (21), compared to the result obtained using the Taylor series expansion, Eq. (7), and with the results obtained with the state of the art parton distribution functions recently obtained in Ref. [22].

Appendix B

We used a code based on the methods developed in Refs. [14,15] to simulate a hard trigger in nucleon–nucleus high energy collisions. The framework is an event–by–event approach, based on nuclei described by specific configurations, *i.e.* nucleons' positions in each event, prepared beforehand with state of the art methods [23,24]. In the case of the deuteron, we obtained a 3D distribution using the well–known Hulthen radial wave function to generate the relative position of the neutron and proton in a probabilistic way, and selected a random orientation of the deuteron with respect to the longitudinal and vertical directions, in each event. We calculated a quantity which depends on the specific configuration, impact parameter, b, and number of wounded nucleons, ν:

$$Z_h(b,\nu) = \int d\boldsymbol{\rho} \sum_{j=1}^{A} \theta(z_{hard} - z_j)\, \frac{1}{\pi B}\, e^{-(\boldsymbol{b}+\boldsymbol{\rho}-\boldsymbol{b}_j)^2/B}\,, \tag{22}$$

where $\boldsymbol{b}$ is the vector impact parameter of the projectile, $\boldsymbol{\rho}$ is the hard interaction point in transverse plane, $\boldsymbol{b}_j$ is the j–th target nucleon position in the transverse plane, and z_{hard} is the z coordinate of the hard–interacting nucleon; the dependence on ν is implicit, here, because we actually build $Z_h(b,\nu)$ as a two–dimensional distribution. Moreover, $\boldsymbol{\rho}$ is integrated because we allow for the hard interaction to occur anywhere in the transverse plane, regardless of the specific nucleon who is interacting.

The quantity in Eq. (22) contains the full dependence on the impact parameter, b, and number of collisions, ν, which we calculated for three nuclei: carbon ^{12}C, copper ^{63}Cu and gold ^{197}Au, as it was implemented this way in the code first developed in Ref. [14]. The final result Z_H is averaged over nuclear configurations, integrated in $\boldsymbol{b}$ and averaged in ν, as follows:

$$Z_H = \frac{\sum_{\nu=1}^{A} \nu \int d\boldsymbol{b}\, \langle Z_h(b,\nu)\rangle_{conf}}{\sum_{\nu=1}^{A} \int d\boldsymbol{b}\, \langle Z_h(b,\nu)\rangle_{conf}}\,, \tag{23}$$

where $\langle ...\rangle_{conf}$ denotes an average over many nucleon configurations [23]. All of the integrations/summations in Eqs. (22) and (23) are shown in the same order they are performed in the code. A sketch of the process described by Eq. (23) is in Fig. 3; results are in Fig. 4.

Appendix C

In this Appendix we describe an approach to estimate isoscalar corrections applied to the experimental data, shown in Fig. 5.

The impulse approximation for the ratio $R(A/D)$ reads as follows:

$$R = \frac{\sigma_A}{N\,\sigma_n + Z\,\sigma_p}\,. \tag{24}$$

The available experimental data of Ref. [7] were reported for

$$U = (2/A)\,(\sigma_A/\sigma_D)\,, \tag{25}$$

and the analysis of Refs. [9,33] finds

$$\frac{\sigma_{pd}}{2\sigma_p} = 1 + \lambda = 1.1 - 1.15\,. \tag{26}$$

Eq. (26) leads to $\sigma_n/\sigma_p = (1+2\lambda) = 1.3$, for $\lambda = 0.15$, with a weak x_A dependence. We can write the ratio R as follows:

$$R = U\,\frac{(\sigma_n+\sigma_p)/2)}{(N/A)\,\sigma_n + Z/A\,\sigma_p}\,. \tag{27}$$

Using Eq. (27), with Z=74, A=184 for tungsten, we find $R(W) = 0.975\ U$. For copper the correction is even smaller, amounting to $R(Cu) = 0.99\ U$. These estimates are applied to the data points in Fig. 5.

References

[1] J.J. Aubert, et al., Measurement of the deuteron structure function $F2$ and a comparison of proton and neutron structure, Phys. Lett. B 123 (1983) 123–126, https://doi.org/10.1016/0370-2693(83)90971-1.

[2] L.L. Frankfurt, M.I. Strikman, High-energy phenomena, short range nuclear structure and QCD, Phys. Rep. 76 (1981) 215–347, https://doi.org/10.1016/0370-1573(81)90129-0.

[3] L.L. Frankfurt, M.I. Strikman, Hard nuclear processes and microscopic nuclear structure, Phys. Rep. 160 (1988) 235–427, https://doi.org/10.1016/0370-1573(88)90179-2.

[4] M. Arneodo, et al., Measurement of the proton and deuteron structure functions, F_2^p and F_2^d, and of the ratio σ_L/σ_T, Nucl. Phys. B 483 (1997) 3–43, https://doi.org/10.1016/S0550-3213(96)00538-X, arXiv:hep-ph/9610231.

[5] A.M. Sirunyan, et al., Constraining gluon distributions in nuclei using dijets in proton–proton and proton–lead collisions at $\sqrt{s_{\rm NN}} = 5.02$ TeV, Phys. Rev. Lett. 121 (6) (2018) 062002, https://doi.org/10.1103/PhysRevLett.121.062002, arXiv:1805.04736.

[6] P.E. Reimer, Exploring the partonic structure of hadrons through the Drell–Yan process, J. Phys. G 34 (2007) S107–S126, https://doi.org/10.1088/0954-3899/34/7/S06, arXiv:0704.3621.

[7] A.S. Tadepalli, Light anti–quark flavor asymmetry in the nucleon sea and the nuclear dependence of anti–quarks in nuclei at the SeaQuest Experiment, Ph.D. thesis, Rutgers U., Piscataway (main), Rutgers U., Piscataway, 2019.

[8] P.L. McGaughey, J.M. Moss, J.C. Peng, High-energy hadron induced dilepton production from nucleons and nuclei, Annu. Rev. Nucl. Part. Sci. 49 (1999) 217–253, https://doi.org/10.1146/annurev.nucl.49.1.217, arXiv:hep-ph/9905409.

[9] J. Dove, B. Kerns, R.E. McClellan, S. Miyasaka, D.H. Morton, K. Nagai, S. Prasad, F. Sanftl, M.B.C. Scott, A.S. Tadepalli, C.A. Aidala, J. Arrington, C. Ayuso, C.L. Barker, C.N. Brown, W.C. Chang, A. Chen, D.C. Christian, B.P. Dannowitz, M. Daugherity, M. Diefenthaler, L.E. Fassi, D.F. Geesaman, R. Gilman, Y. Goto, L. Guo, R. Guo, T.J. Hague, R.J. Holt, D. Isenhower, E.R. Kinney, N. Kitts, A. Klein, D.W. Kleinjan, Y. Kudo, C. Leung, P.-J. Lin, K. Liu, M.X. Liu, W. Lorenzon, N.C.R. Makins, M.M. de Medeiros, P.L. McGaughey, Y. Miyachi, I. Mooney, K. Nakahara, K. Nakano, S. Nara, J.-C. Peng, A.J. Puckett, B.J. Ramson, P.E. Reimer, J.G. Rubin, S. Sawada, T. Sawada, T.-A. Shibata, D. Su, M. Teo, B.G. Tice, R.S. Towell, S. Uemura, S. Watson, S.G. Wang, A.B. Wickes, J. Wu, Z. Xi, Z. Ye, The asymmetry of antimatter in the proton, Nature 590 (2021) 561–565, https://doi.org/10.1038/s41586-021-03282-z.

[10] A. Accardi, X. Jing, J.F. Owens, S. Park, Light quark and antiquark constraints from new electroweak data, 3 2023, arXiv:2303.11509.

[11] F.E. Close, R.G. Roberts, G.G. Ross, The effect of confinement size on nuclear structure functions, Phys. Lett. B 129 (5) (1983) 346–350, https://doi.org/10.1016/0370-2693(83)90679-2.

[12] F.E. Close, R.L. Jaffe, R.G. Roberts, G.G. Ross, Change of confinement scale in nuclei: predictions for structure functions confront electroproduction data, Phys. Rev. D 31 (1985) 1004–1013, https://doi.org/10.1103/PhysRevD.31.1004.

[13] L.L. Frankfurt, M.I. Strikman, Point–like configurations in hadrons and nuclei and deep inelastic reactions with leptons: EMC and EMC–like effects, Nucl. Phys. B 250 (1985) 143–176, https://doi.org/10.1016/0550-3213(85)90477-8.

[14] M. Alvioli, B.A. Cole, L. Frankfurt, D.V. Perepelitsa, M. Strikman, Evidence for x–dependent proton color fluctuations in pA collisions at the CERN large hadron collider, Phys. Rev. C 93 (1) (2016) 011902, https://doi.org/10.1103/PhysRevC.93.011902, arXiv:1409.7381.

[15] M. Alvioli, L. Frankfurt, D. Perepelitsa, M. Strikman, Global analysis of color fluctuation effects in proton– and deuteron–nucleus collisions at RHIC and the LHC, Phys. Rev. D 98 (7) (2018) 071502, https://doi.org/10.1103/PhysRevD.98.071502, arXiv:1709.04993.

[16] J. Collins, Foundations of Perturbative QCD, Cambridge Monographs on Particle Physics, Nuclear Physics and Cosmology, vol. 32, Cambridge University Press, 2011.

[17] C. Ciofi degli Atti, S. Simula, Realistic model of the nucleon spectral function in few and many nucleon systems, Phys. Rev. C 53 (1996) 1689, https://doi.org/10.1103/PhysRevC.53.1689, arXiv:nucl-th/9507024.

[18] C. Ciofi degli Atti, S. Simula, L.L. Frankfurt, M.I. Strikman, Two nucleon correlations and the structure of the nucleon spectral function at high values of momentum and removal energy, Phys. Rev. C 44 (1991) R7–R11, https://doi.org/10.1103/PhysRevC.44.R7.

[19] M. Alvioli, C. Ciofi degli Atti, I. Marchino, V. Palli, H. Morita, Effects of ground–state correlations on high energy scattering off nuclei: the case of the total neutron–nucleus cross section, Phys. Rev. C 78 (2008) 031601, https://doi.org/10.1103/PhysRevC.78.031601, arXiv:0807.0873.

[20] M. Alvioli, C. Ciofi degli Atti, H. Morita, Universality of nucleon–nucleon short–range correlations: the factorization property of the nuclear wave function, the relative and center–of–mass momentum distributions, and the nuclear contacts, Phys. Rev. C 94 (4) (2016) 044309, https://doi.org/10.1103/PhysRevC.94.044309, arXiv:1607.04103.

[21] O. Hen, G.A. Miller, E. Piasetzky, L.B. Weinstein, Nucleon–nucleon correlations, short–lived excitations, and the quarks within, Rev. Mod. Phys. 89 (4) (2017) 045002, https://doi.org/10.1103/RevModPhys.89.045002, arXiv:1611.09748.

[22] T.-J. Hou, J. Gao, T.J. Hobbs, K. Xie, S. Dulat, M. Guzzi, J. Huston, P. Nadolsky, J. Pumplin, C. Schmidt, I. Sitiwaldi, D. Stump, C.-P. Yuan, New CTEQ global analysis of quantum chromodynamics with high–precision data from the LHC, Phys. Rev. D 103 (2021) 014013, https://doi.org/10.1103/PhysRevD.103.014013.

[23] M. Alvioli, H.-J. Drescher, M. Strikman, A Monte Carlo generator of nucleon configurations in complex nuclei including Nucleon–Nucleon correlations, Phys. Lett. B 680 (2009) 225–230, https://doi.org/10.1016/j.physletb.2009.08.067, arXiv:0905.2670.

[24] M. Alvioli, M. Strikman, Spin–isospin correlated configurations in complex nuclei and neutron skin effect in $W^{\pm}$ production in high–energy proton–lead collisions, Phys. Rev. C 100 (2) (2019) 024912, https://doi.org/10.1103/PhysRevC.100.024912, arXiv:1811.10078.

[25] J. Hammelmann, A. Soto-Ontoso, M. Alvioli, H. Elfner, M. Strikman, Influence of the neutron–skin effect on nuclear isobar collisions at energies available at the BNL relativistic heavy ion collider, Phys. Rev. C 101 (6) (2020) 061901, https://doi.org/10.1103/PhysRevC.101.061901, arXiv:1908.10231.

[26] J. Arrington, J. Bane, A. Daniel, N. Fomin, D. Gaskell, J. Seely, R. Asaturyan, F. Benmokhtar, W. Boeglin, P. Bosted, M.H.S. Bukhari, M.E. Christy, S. Connell, M.M. Dalton, D. Day, J. Dunne, D. Dutta, L. El Fassi, R. Ent, H. Fenker, H. Gao, R.J. Holt, T. Horn, E. Hungerford, M.K. Jones, J. Jourdan, N. Kalantarians, C.E. Keppel, D. Kiselev, A.F. Lung, S. Malace, D.G. Meekins, T. Mertens, H. Mkrtchyan, G. Niculescu, I. Niculescu, D.H. Potterveld, C. Perdrisat, V. Punjabi, X. Qian, P.E. Reimer, J. Roche, V.M. Rodriguez, O. Rondon, E. Schulte, K. Slifer, G.R. Smith, P. Solvignon, V. Tadevosyan, L. Tang, G. Testa, R. Trojer, V. Tvaskis, F.R. Wesselmann, S.A. Wood, L. Yuan, X. Zheng, Measurement of the EMC effect in light and heavy nuclei, Phys. Rev. C 104 (2021) 065203, https://doi.org/10.1103/PhysRevC.104.065203.

[27] J. Gomez, R.G. Arnold, P.E. Bosted, C.C. Chang, A.T. Katramatou, G.G. Petratos, A.A. Rahbar, S.E. Rock, A.F. Sill, Z.M. Szalata, A. Bodek, N. Giokaris, D.J. Sherden, B.A. Mecking, R.M. Lombard-Nelsen, Measurement of the A dependence of deep–inelastic electron scattering, Phys. Rev. D 49 (1994) 4348–4372, https://doi.org/10.1103/PhysRevD.49.4348.

[28] L.L. Frankfurt, M.I. Strikman, D.B. Day, M. Sargsyan, Evidence for short–range correlations from high q^2 (e,e′) reactions, Phys. Rev. C 48 (1993) 2451–2461, https://doi.org/10.1103/PhysRevC.48.2451.

[29] N. Fomin, J. Arrington, R. Asaturyan, F. Benmokhtar, W. Boeglin, P. Bosted, A. Bruell, M.H.S. Bukhari, M.E. Christy, E. Chudakov, B. Clasie, S.H. Connell, M.M. Dalton, A. Daniel, D.B. Day, D. Dutta, R. Ent, L. El Fassi, H. Fenker, B.W. Filippone, K. Garrow, D. Gaskell, C. Hill, R.J. Holt, T. Horn, M.K. Jones, J. Jourdan, N. Kalantarians, C.E. Keppel, D. Kiselev, M. Kotulla, R. Lindgren, A.F. Lung, S. Malace, P. Markowitz, P. McKee, D.G. Meekins, H. Mkrtchyan, T. Navasardyan, G. Niculescu, A.K. Opper, C. Perdrisat, D.H. Potterveld, V. Punjabi, X. Qian, P.E. Reimer, J. Roche, V.M. Rodriguez, O. Rondon, E. Schulte, J. Seely, E. Segbefia, K. Slifer, G.R. Smith, P. Solvignon, V. Tadevosyan, S. Tajima, L. Tang, G. Testa, R. Trojer, V. Tvaskis, W.F. Vulcan, C. Wasko, F.R. Wesselmann, S.A. Wood, J. Wright, X. Zheng, New measurements of high-momentum nucleons and short-range structures in nuclei, Phys. Rev. Lett. 108 (2012) 092502, https://doi.org/10.1103/PhysRevLett.108.092502.

[30] M. Alvioli, C. Ciofi degli Atti, L.P. Kaptari, C.B. Mezzetti, H. Morita, Nucleon momentum distributions, their spin–isospin dependence, and short–range correlations, Phys. Rev. C 87 (2013) 034603, https://doi.org/10.1103/PhysRevC.87.034603.

[31] J. Arrington, A. Daniel, D. Day, N. Fomin, D. Gaskell, P. Solvignon, A detailed study of the nuclear dependence of the EMC effect and short–range correlations, Phys. Rev. C 86 (2012) 065204, https://doi.org/10.1103/PhysRevC.86.065204.

[32] R.B. Wiringa, V.G.J. Stoks, R. Schiavilla, Accurate nucleon–nucleon potential with charge–independence breaking, Phys. Rev. C 51 (1995) 38–51, https://doi.org/10.1103/PhysRevC.51.38.

[33] J. Dove, B. Kerns, C. Leung, R.E. McClellan, S. Miyasaka, D.H. Morton, K. Nagai, S. Prasad, F. Sanftl, M.B.C. Scott, A.S. Tadepalli, C.A. Aidala, J. Arrington, C. Ayuso, C.T. Barker, C.N. Brown, T.H. Chang, W.C. Chang, A. Chen, D.C. Christian, B.P. Dannowitz, M. Daugherity, M. Diefenthaler, L.E. Fassi, D.F. Geesaman, R. Gilman, Y. Goto, L. Guo, R. Guo, T.J. Hague, R.J. Holt, D. Isenhower, E.R. Kinney, N.D. Kitts, A. Klein, D.W. Kleinjan, Y. Kudo, P.J. Lin, K. Liu, M.X. Liu, W. Lorenzon, N.C.R. Makins, M.M. de Medeiros, P.L. McGaughey, Y. Miyachi, I. Mooney, K. Nakahara, K. Nakano, S. Nara, J.C. Peng, A.J. Puckett, B.J. Ramson, P.E. Reimer, J.G. Rubin, S. Sawada, T. Sawada, T.A. Shibata, S.H. Shiu, D. Su, M. Teo, B.G. Tice, R.S. Towell, S. Uemura, T.S. Watson, S.G. Wang, A.B. Wickes, J. Wu, Z. Xi, Z. Ye, Measurement of flavor asymmetry of light–quark sea in the proton with Drell–Yan dimuon production in $p+p$ and $p+d$ collisions at 120 GeV, 2022, https://doi.org/10.48550/ARXIV.2212.12160.